

# Strike the Balance: On-the-Fly Uncertainty based User Interactions for Long-Term Video Object Segmentation

Stéphane Vujasinović<sup>✉</sup>, Stefan Becker<sup>✉</sup>, Sebastian Bullinger<sup>✉</sup>, Norbert Scherer-Negenborn, and Michael Arens<sup>✉</sup>

Fraunhofer IOSB, Ettlingen, Germany  
{name}.{surname}@iosb.fraunhofer.de

**Abstract.** In this paper, we introduce a variant of video object segmentation (VOS) that bridges interactive and semi-automatic approaches, termed Lazy Video Object Segmentation (ziVOS). In contrast, to both tasks, which handle video object segmentation in an off-line manner (*i.e.*, pre-recorded sequences), we propose through ziVOS to target on-line recorded sequences. Here, we strive to strike a balance between performance and robustness for long-term scenarios by soliciting user feedback’s on-the-fly during the segmentation process. Hence, we aim to maximize the tracking duration of an object of interest, while requiring minimal user corrections to maintain tracking over an extended period. We propose a competitive baseline, *i.e.*, Lazy-XMem, as a reference for future works in ziVOS. Our proposed approach uses an uncertainty estimation of the tracking state to determine whether a user interaction is necessary to refine the model’s prediction. To quantitatively assess the performance of our method and the user’s workload, we introduce complementary metrics alongside those already established in the field. We evaluate our approach using the recently introduced LVOS dataset, which offers numerous long-term videos. Our code is publicly available at <https://github.com/Vujas-Eteph/LazyXMem>.

## 1 Introduction

Video Object Segmentation (VOS) is a fundamental and challenging problem that encompasses numerous tasks [84], including, among others, semi-automatic Video Object Segmentation (sVOS) and interactive Video Object Segmentation (iVOS). In sVOS, given an initial segmentation mask for the first video frame, methods classify each pixel in the subsequent video frames as a part of the object of interest (*i.e.*, foreground) or the background. Here, a user only interacts at the start of the sequence by providing the corresponding annotation mask to indicate which object to segment in the video. In contrast, iVOS methods incorporate user interactions in a multi-round scheme, where the user interacts with the method before each round, to improve the segmentation quality on the subsequent rounds. Both applications are suited for pre-recorded sequences,

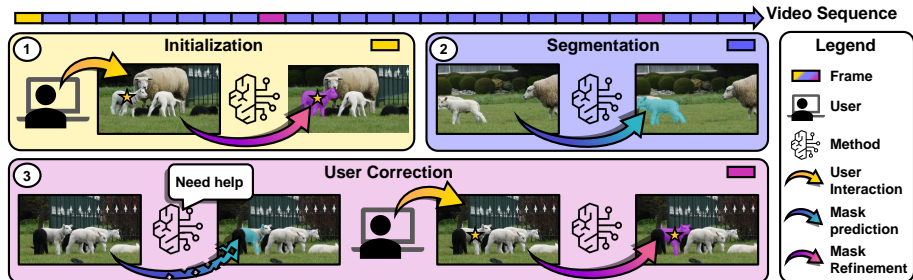


**Fig. 1:** Visual representation of the ziVOS framework. (1) The user initiates the segmentation by clicking to identify the object of interest in the video, (2) thus indicating which object to segment. Only when requested by the method (3) does the user provides corrective clicks on-the-fly.

*i.e.*, offline segmentation, as sVOS methods assumes that the user has unlimited time to annotate the initial frame with utmost accuracy, whereas iVOS approaches expect the user to inspect the segmentation quality of the previous round, and interact for multiple rounds until the desired segmentation quality is achieved. However, while sVOS methods demonstrate impressive performances on short-term datasets [49, 70], their applicability to long-term sequences remains under-explored [2, 6, 8, 22, 36, 38, 60, 75] and yet to be addressed by iVOS methods. This underscores a gap in methodologies suited for prolonged sequences, where maintaining error-free segmentation under challenging conditions becomes increasingly difficult.

In this paper, we explore a hybrid framework, named *lazy interactive Video Object Segmentation* (ziVOS) (depicted in Figure 1), that bridges the methodologies of sVOS and iVOS, focusing on maintaining robust object tracking with minimal user interactions. Unlike iVOS, we discard the round based scheme and integrate user corrections on-the-fly, refining the model’s prediction as needed, while the method segments the video. Moreover, distinct from sVOS, in ziVOS the object of interest is indicated with a user interaction (*i.e.*, click). To achieve this, we only allow one interaction per frame and per object, and solely rely on click-based interactions, as pointing an object is the quickest, most intuitive and predictable interaction type for humans [14, 18]. Hence, we propose ziVOS to emulate a human-in-the-loop process when segmenting a video in an online fashion, that is better suited for dynamic applications, where user engagement is feasible and where maintaining consistent object tracking in challenging conditions is more critical than achieving segmentation accuracy. Concretely, our objective shifts from segmenting an object with high accuracy to maximizing the number of frames in which the object is segmented above a minimal alignment ratio (*i.e.*, Intersection over Union (IoU)), denoted as  $\tau_{\text{iou}}$ , by integrating user corrections on-the-fly (only at critical events), while simultaneously reducing the user’s workload.

We propose Lazy-XMem, as a baseline for future works addressing ziVOS. Lazy-XMem assess the uncertainty of a predicted object mask on-the-fly and refines it accordingly (through SAM-HQ [29]), if the uncertainty is too high, through either pseudo-corrections or user-corrections. In our approach, entropy [53] serves as a proxy to estimate the performance of the tracking state (*i.e.*, how the predicted mask would align with a hypothetical ground-truth).

Similarly, recent studies in iVOS [15, 76] evaluate which frame to interact with at the end of a round. They compare the embeddings of each frame in the video sequence against all other frame embeddings to determine which frame to suggest to the user for new interactions, limiting this strategy to only pre-recorded videos. In contrast, our criterion is solely defined w.r.t. the tracker’s state, how accurate the prediction is for the current observed frame, allowing us to work with non-pre-recorded sequences. To our knowledge, only QDMN by Liu *et al.* [38] also estimates the tracking state in an online fashion, by predicting a quality score through a second head (following a similar design to [24]). However, unlike prior works [15, 38, 76], we estimate the tracker’s state on pixel level, eliminating the need to train a second head. An additional benefit, to computing the uncertainty on pixel-level is that we can visually indicate ambiguous regions to the user where an interaction might be the most helpful. Moreover, depending on the confidence of the predicted mask, Lazy-XMem decides whether the current predicted mask will be stored in the memory. Hence, by selectively refining masks based on entropy-driven uncertainty estimation, we aim to maintain a balance between robustness and user-workload in ziVOS, specifically in long-term scenarios.

In this context the paper presents the following contributions: (1) Online (on-the-fly) assessment of the tracking state quality, by leverage entropy, to minimize the user’s monitoring by providing interactions only at critical events (*e.g.*, occlusions, distractors). (2) A scheme to integrate pseudo-interactions, into our interactive feed-back loop to reduce the user’s workload. We generate pseudo-interactions based on the original mask and the corresponding uncertainty. (3) Suitable metrics to evaluate the robustness of our method, and the user’s workload w.r.t. the standard  $\mathcal{J}\&\mathcal{F}$  metric proposed by Perazzi *et al.* [47]. (4) Evaluation on long-term [22] sequences to highlight the suitability of our method to maintain robust tracks.

## 2 Related Work

### 2.1 Semi-Automatic Video Object Segmentation

Early deep learning methods in sVOS follow an *online fine-tuning approach* [4, 39, 42, 59, 65, 66], which adapts the network’s parameters on-the-fly while segmenting the objects of interest in the video sequence. This results, in slow inference times and poor generalization capabilities [84]. Concurrently, *propagation-based methods* [23, 26, 28, 48, 81] propagate the masks from the previous adjacent frame to the current one for segmentation, but they are prone to error accumulation and often fail during occlusions [84]. *Matching-based meth-*

*ods* [13, 58, 72–75, 78] leverage features from the initial and previous adjacent frame to segment the current frame. The leading methods in the field further integrate features from in-between frames (previously processed) into an external memory [9, 10, 37, 45, 46, 51, 52, 67, 73, 75], using cross-attention to link features from previous frames to the current frame to segment. However, these methods are limited in real-world applications due to their expanding memory requirements, making long-term segmentation on consumer-grade GPUs challenging.

Recent works address this bottleneck by selectively integrating frame representations into the external memory [33, 38, 60] or by generating compact representations to summarize similar features together [2, 6, 8, 34, 36]. These methods effectively manage the memory footprint, enabling more efficient sVOS on long-term videos. Newer methods [6] also explore improved ways to differentiate similar objects (distractors) from each other. Additionally, new datasets have recently been introduced [1, 16, 22] to provide an alternative to the classical DAVIS [49] and YouTube-VOS [70] datasets, with some targeted specifically for long-term video segmentation [22, 36] and tracking [32].

Contemporary works [11, 71, 85] leverage Segment Anything Model (SAM) [30] or a variant [29, 79, 83] to refine the original mask predicted by an sVOS baseline [8, 75]. However, in contrast to our framework, they refine every  $n$ -th mask predicted by the sVOS backbone with a SAM based approach [29, 30, 79, 83], and require continuous user monitoring to identify when interventions are needed. Furthermore, they diminish the influence to enhance the predictive accuracy for subsequent frame as they do not update the memory with the refined mask.

## 2.2 Interactive Image Segmentation

In interactive Image Object Segmentation (iIOS), methods predict a mask for an object of interest based on user interactions for a single image. These approaches aim to reduce the user’s workload by replacing densely annotated mask for sparse annotations (*e.g.*, clicks [19, 27, 31, 35, 54, 55, 69], extreme points [17, 40, 82], or bounding boxes [50, 64, 68]). Most notable approach is f-BRS [54] which optimizes internal auxiliary features of the segmentation network to align its prediction’s at the clicked position with the user annotated label. A follow up work by Sofiiuk *et al.* [55], replaces the previous f-BRS backbone with an HRNet [62] + OCR [77] network, to maintain high quality features through out the network to obtain a preciser segmentation mask. Since the introduction of SAM [30], a plethora of SAM-based methods have been proposed to solve the task in medical imaging [41] and natural images [80]. For instance, SAM-HQ [29] improves upon SAM by better handling complex shapes, such as thinner structures and objects with holes. Additionally, faster approaches like FastSAM [83] and MobileFast [79] have been developed to enhance performance and efficiency.

## 2.3 Interactive Video Object Segmentation

Originally intended to reduce the user’s workload during video annotations [5], iVOS methods integrate user interactions in a round-based process. Most ap-

proaches follow the design introduced by Benard *et al.* [3], which combines sVOS and iIOS pipelines. The blueprint process for the iVOS task is as follow: (1) Firstly, the method predicts a segmentation mask for each frame in the video (through a sVOS baseline), based on an initial mask provided for a frame. (2) Next, a user scrolls through the resulting masks and selects a frame to interact with (*e.g.*, through clicks [25, 61, 63], scribbles [9, 20, 21, 43, 44]). Based on the provided interaction, a new mask is predicted for the annotated frame, serving as a new starting point when repeating step (1). Steps (1) and (2) are repeated one after the other, until the user is satisfied with the final results.

A persistent bottleneck is determining which frame to annotate for the next round. Recent approaches address this by identifying a quartet of candidate frames for the user to annotate [21], estimating which frame would yield the most improvement [76], or using a weakly supervised method to indicate the frame and type of interaction [15] to the user. To determine which frame or set of frames to annotate, these methods map each frame in the sequence into an embedding space, restricting them to short videos, as it requires storing the embedding of every frame. Here, each embedding encode the frame’s representation and the quality of the corresponding predicted mask. The best candidate frame is selected by comparing each embedding w.r.t. others and against those of annotated frames, either through an agent [76] or by choosing the embedding that is furthest from any annotated embedding [15]. In contrast, our approach introduces corrections on-the-fly by directly assessing the tracking state during segmentation, thereby proposing an online methodology that is also not restricted to short sequences.

## 2.4 Uncertainty Estimation in Video Object Segmentation

Uncertainty estimations is essential to improve the reliability and explainability of a model, however estimating the uncertainty of Deep Neural Networks (DNNs), remains a challenging topic. To our knowledge, only the work by Liu *et al.* [38] incorporates a confidence score to asses the tracking state on-the-fly for the sVOS task by leveraging an auxiliary head (*i.e.*, QAM module), predicting a confidence score on how likely the predicted mask would align with a ground-truth annotation. Similar to our approach, QDMN manages its memory updates based on a threshold value that determines whether a predicted mask, given its confidence level, is reliable enough to be stored in the external memory. However, as the QAM module only predicts a single score per object, it is unable to guide the user during an interaction, as to where a correction might be the most valuable. In contrast, we explore uncertainty estimation through information theory [53] (*i.e.*, entropy) and update the memory with the refined mask.

## 3 Method

We present Lazy-XMem, depicted in Figure 2, as a baseline for future works targeting ziVOS. Lazy-XMem comprises the following key components: (1) An

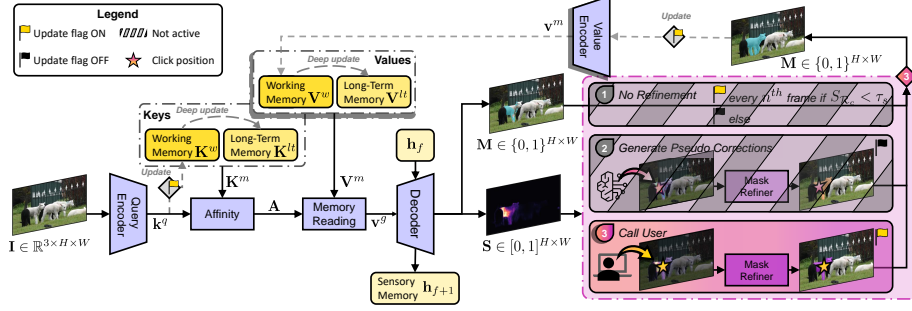


**Fig. 2:** Overview of Lazy-XMLM for Lazy Video Object Segmentation. Our method relies on an sVOS baseline (*i.e.*, XMem [8]). We leverage the entropy to estimate on-the-fly the tracking state. Based on the tracking state’s, the method either uses the original mask of the sVOS baseline, or refine the original mask by generating pseudo-interactions, or requesting user interaction.

sVOS baseline, to predict object masks; (2) An uncertainty assessment component; (3) A mask refiner, to refine the original prediction from the sVOS baseline; (4) An interaction-issuer, to issue either pseudo- or user-corrections and (5) a memory update mechanism.

### 3.1 XMem as Baseline

We rely on XMem [8] as our sVOS baseline. Initialized with an object mask at the beginning, the network predicts object masks on the subsequent frames. In the following, we assume the network to segment a single object for ease of notations. The key components are:

**Convolutional Blocks:** (1) A *query encoder*, extracting query key features  $\mathbf{k}^q \in \mathbb{R}^{C_k \times \frac{H}{16} \times \frac{W}{16}}$  from the current image to segment. (2) A *decoder*, predicting an object mask  $\mathbf{M} \in \{0,1\}^{H \times W}$  for a query frame  $\mathbf{I} \in \mathbb{R}^{3 \times H \times W}$ . (3) Lastly, a *value encoder*, that extracts value features  $\mathbf{v}^m \in \mathbb{R}^{C_v \times \frac{H}{16} \times \frac{W}{16}}$  based on the current image  $\mathbf{I}$  and the predicted mask  $\mathbf{M}$ .

**Memories:** In contrast to previous works [9, 10, 45], XMem [8] uses three distinct memories: a *working*-, a *long-term*-, and a *sensory*-memory. Each memory encodes different information to avoid redundancy.

(1) The *working* memory, based on the design of matching-based approaches [10], is updated every  $n^{\text{th}}$  frame with the corresponding query and value representations in  $\mathbf{K}^w \in \mathbb{R}^{C_k \times t \times \frac{H}{16} \times \frac{W}{16}}$  and  $\mathbf{V}^w \in \mathbb{R}^{C_v \times t \times \frac{H}{16} \times \frac{W}{16}}$ . Specifically, the memory is filled with the high resolution queries keys  $\mathbf{k}^q$  as memory keys  $\mathbf{k}^m$  and the associated values  $\mathbf{v}^m$  respectively until the representations in the memory reach  $t = T_{max}$ .

(2) Once the working memory reaches full capacity (*i.e.*,  $t = T_{max}$ ), the representations in  $\mathbf{K}^w$  and  $\mathbf{V}^w$ , where  $t \in \{1, T_{max} - 1\}$ , are extracted into  $l$  prototypes features  $\mathbf{k}^p \in \mathbb{R}^{C_k \times l}$  and  $\mathbf{v}^p \in \mathbb{R}^{C_v \times l}$ . The key-values pairs converted from the working memory to prototypes are selected based on how often they are

solicited during the *memory read operation*. Hence the long-term memory for the keys-prototypes is updated by concatenating  $\mathbf{k}^p$  to  $\mathbf{K}^{lt} \in \mathbb{R}^{C_k \times L}$ , and similarly for the value prototypes  $\mathbf{v}^p$  into  $\mathbf{V}^{lt} \in \mathbb{R}^{C_v \times L}$ . As the long-term continuously accumulates prototypes, a least-frequent-usage (LFU [8, 36]) filtering is used to remove obsolete features, not used after a certain period.

(3) Finally the sensory memory, *i.e.*, two GRU cells [12], update a hidden representation  $\mathbf{h}_f \in \mathbb{R}^{C_h \times \frac{H}{16} \times \frac{W}{16}}$ . The hidden representation is updated every frame with the first GRU and encodes prior information such as position [8], while the cell updates the hidden representation only whenever the working memory reaches full capacity, to delete redundant information between the hidden representation and the working-memory [8].

**Memory Reading:** During the memory reading operation, the memory elements used during matching are taken from the working and long-term memory, resulting in a memory of size  $N = T \frac{H}{16} \frac{W}{16} + L$ . The similarity function used to match memory keys with query keys is based on the *anisotropic l2-similarity function* [8]. The similarity matrix  $\mathbf{W}(\mathbf{K}^m, \mathbf{k}^q) \in \mathbb{R}^{N \times \frac{H}{16} \frac{W}{16}}$ , encodes the similarity between the  $i$ -th key feature in the memory (working and long-term) and the  $j$ -th key in the query representation. After computing  $\mathbf{W}$ , the model applies a softmax operation along the memory (*i.e.*, the rows), resulting in the affinity matrix  $\mathbf{A}$ . During the memory readout operation, the model leverages  $\mathbf{A}$  to weight the memory values, to generate a new value  $\mathbf{v}^g \in \mathbb{R}^{C_v \times \frac{H}{16} \frac{W}{16}}$  (only used by the decoder) through

$$\mathbf{v}^g = (\mathbf{V}^m)^\top \mathbf{A}(\mathbf{K}^m, \mathbf{k}^q), \quad (1)$$

where  $\mathbf{K}^m \in \mathbb{R}^{C_k \times N}$  is simply the concatenation of the  $\mathbf{K}^w$  with the  $\mathbf{K}^{lt}$  (*i.e.*,  $\mathbf{K}^m = \mathbf{K}^w \oplus \mathbf{K}^{lt}$ , where  $\oplus$  denotes the concatenation) along the row. Similarly we obtain  $\mathbf{V}^m \in \mathbb{R}^{C_v \times N}$ . The keys encode robust semantic information to appearance variations, useful during the memory read operation (*i.e.*, cross-attention), while values encode boundary and texture cues [45], needed in the decoding stage.

### 3.2 Uncertainty Estimation via Entropy

To estimate the uncertainty of the tracking state (*i.e.*, the predicted segmentation mask), we leverage entropy [53], denoted as  $S$ . We consider pixels as discrete random variables whose classes  $c$  belong to the set  $\mathcal{C}$ , where  $\mathcal{C}$  contains every object observed in a given video, including the background (*i.e.*,  $c = 0$ ). We use the output values of the softmax layer as a probability mass functions  $p_{\mathcal{C}}(c | x_{h,w})$  for each pixel located  $x$  at  $(h, w)$ . Here,  $c \in \mathcal{C}$  denotes the class of the pixel, and  $(h, w)$  specifies the pixel's location in terms of height  $h$  and width  $w$  within a mask  $\mathbf{M} \in \{0, \dots, |\mathcal{C}|\}^{H \times W}$ .

However, as the number of classes  $|\mathcal{C}|$  can vary over time (*i.e.*, from one video to another, or even from one frame to another in the same video), we normalize the entropy for consistency and comparability. Hence, we express the entropy of

a pixel  $x_{h,w}$  by

$$\mathbf{S}_{h,w} = -\frac{\sum_{c \in \mathcal{C}} p_{\mathcal{C}}(c | x_{h,w}) \log(p_{\mathcal{C}}(c | x_{h,w}))}{\log(|\mathcal{C}|)}, \quad (2)$$

where  $\mathbf{S} \in [0, 1]^{H \times W}$  denotes the corresponding entropy map of the current frame to segment.

To compute the entropy (*i.e.*, uncertainty) for a specific object class  $c$ , we use a dilated mask  $\mathbf{M}_c^d$  based on the original object mask  $\mathbf{M}_c$ , such that the dilated mask allows us to exclude the background, while still considering the uncertainty around the predicted object’s edges. Otherwise, using directly the predicted mask  $\mathbf{M}_c$  might truncate the aleatoric uncertainty (especially near the edges of the object). Hence, we define a region  $\mathcal{R}_c = \{(h, w) \mid \mathbf{M}_c^d(h, w) = 1\}$ , such that through

$$S_{\mathcal{R}_c} = \sum_{r \in \mathcal{R}_c} \mathbf{S}_r(x_r \mid x_{r-1}, \dots, x_1) \approx \sum_{r \in \mathcal{R}_c} \mathbf{S}_r, \quad (3)$$

we compute the joint entropy within the considered object region (we investigate different values for the dilated mask in our supplementary material). However, computing the joint entropy is impractical as the network does not provide any joint or conditional distributions for a formal evaluation. Additionally, the computational cost would grow exponentially with respect to the number of classes  $\mathcal{C}$  and the size of the region  $\mathcal{R}_c$  (*i.e.*,  $O(|\mathcal{C}|^{|\mathcal{R}_c|})$  time complexity). To reduce the computational complexity, we assume zero mutual information between the predicted probability distributions of pixels in the region  $\mathcal{R}_c$ . This allows us to sum the entropy of each pixel  $\mathbf{S}_{h,w}$  belonging to the region of interest  $\mathbf{M}_c^d$  (refer to Eq. (3)), allowing us to significantly reduce the computational cost (*i.e.*, to  $O(|\mathcal{C}| \times |\mathcal{R}_c|)$  complexity).

Additionally, considering that the object size may vary from one image to another, we divide  $S_{\mathcal{R}_c}$  by the size of the corresponding region  $|\mathcal{R}_c|$ . This dampens the fluctuation of  $S_{\mathcal{R}_c}$  due to object size variations. Thus, we effectively assess the uncertainty for a predicted mask  $\mathbf{M}_c$  (*i.e.*, on object level) through  $S_{\mathcal{R}_c}$ .

### 3.3 Mask Refinement

For the mask-refinement component, we rely on SAM-HQ [29], which extends SAM [30] to segment intricate object structures in more details, while preserving its zero-shot capabilities and flexibility. SAM-HQ [29] introduces two additional components on top of SAM [30]: (1) An *HQ-output token* to correct the original SAM’s mask. (2) A *global-local features fusion*, which fuses early features with later ones (*i.e.*, after the first and last global attention block respectively) to enrich the features used by the mask decoder. For more details about SAM [30] and SAM-HQ [29] we refer the reader to the original sources.



### 3.4 Issuing Corrections

For a given object  $c$ , we record the corresponding masked entropy  $S_{\mathcal{R}_c}$  at each frame, such that  $\mathbf{s}_{\mathcal{R}_c} = [S_{\mathcal{R}_c}(f = 0), \dots, S_{\mathcal{R}_c}(f = F)]$ , where  $f$  denotes the frame index and  $F$  the latest frame to segment. Let  $\mathbf{s}'_{\mathcal{R}_c}$  denote the derivative of  $\mathbf{s}_{\mathcal{R}_c}$ , such that  $\mathbf{s}'_{\mathcal{R}_c} = [\Delta S_{\mathcal{R}_c}(f = 1), \dots, \Delta S_{\mathcal{R}_c}(f = F)]$ , where  $\Delta S_{\mathcal{R}_c}(f) = S_{\mathcal{R}_c}(f) - S_{\mathcal{R}_c}(f - 1)$ . Depending on  $\Delta S_{\mathcal{R}_c}(F)$  we either generate a pseudo- or request a user-correction.

**User-Correction:** A user correction is prompted whenever  $\Delta S_{\mathcal{R}_c}(f) \geq \tau_u$ , where  $\tau_u$  denotes the threshold above which a user correction is requested. The user indicates a foreground or background region via a positive or negative click, which is then processed by the mask refiner to generate a new mask. The original mask is not used during refinement due to its high uncertainty.

**Pseudo-Correction:** In addition to requesting on-the-fly user corrections, the model generates pseudo-corrections when  $\tau_u > \Delta S_{\mathcal{R}_c}(f) \geq \tau_p$ , with  $\tau_p$  representing the lower bound for a pseudo-correction to be generated. A pseudo-correction  $p_f^c$  for object  $c$ , given frame  $f$ , is by

$$\mathbf{E}_c(h, w) = \min_{(h_r, w_r) \in \Omega} \sqrt{(h - h_r)^2 + (w - w_r)^2}, \quad (4)$$

$$p_f^c = \operatorname{argmax}_{(h, w)} (\mathbf{M}_c^d \odot \mathbf{E}_c \odot (\mathbf{1}_{H \times W} - \mathbf{S})), \quad (5)$$

where  $\Omega$  denotes the set of pixel that belong to the boundaries of the object mask  $\mathbf{M}_c$ ,  $\mathbf{E}_c$  a distance field, and  $\odot$  represents the Hadamard product.

### 3.5 Interaction and Uncertainty Driven Memory Updates

At each user-correction, we update the working memory of our sVOS baseline with the newly refined mask. This update strategy, termed *Interaction-Driven Update* (IDU), improves the method’s robustness as the refined mask can influence the segmentation of the subsequent frames. An additional update mechanism, named *Uncertainty-Driven Update* (UDU), prevents updating the working memory with the original representation when the corresponding uncertainty  $S_{\mathcal{R}_c}$ , exceeds  $\tau_m$  (similarly to QDMN [38]).

## 4 Metrics

Since we introduce ziVOS, we propose complementary metrics to the standard  $\mathcal{J}\&\mathcal{F}$  presented by Perazzi *et al.* [47] to quantify the user’s workload in providing on-the-fly corrections and to evaluate the robustness of a given method.

### 4.1 Robustness Metric

We take inspiration from Kristan *et al.* [32] and propose  $\mathbf{R}@_{\tau_{\text{IoU}}}$  (higher is better) to measure the robustness of a method. Given a threshold value  $\tau_{\text{IoU}}$ , we

compute the ratio of frames, in which the predicted object mask attains an IoU above or equal to  $\tau_{IoU}$  for all objects in a given dataset. More formally, let  $\mathcal{O}$  be the set of objects in the dataset, where  $F_o$  represents the number of frames in which object  $o$  is present, we define  $R@_{\tau_{IoU}}$ , such that

$$R@_{\tau_{IoU}} \triangleq \frac{1}{|\mathcal{O}|} \sum_{o \in \mathcal{O}} \frac{1}{|F_o|} \sum_{f \in F_o} \mathbb{1}_{[\text{IoU}(\mathbf{M}_f^o, \mathbf{GT}_f^o) \geq \tau_{IoU}]}, \quad (6)$$

where  $\mathbf{M}_f^o$  and  $\mathbf{GT}_f^o$  denote respectively the predicted mask and ground-truth annotation for object  $o$  at frame  $f$ . Like in [32], whenever the method correctly predicts the absence of an object we set  $\mathbb{1}_{\text{IoU}(\mathbf{M}_f^o, \mathbf{GT}_f^o) \geq \tau_{IoU}}$  to 1, otherwise to 0.

## 4.2 User-Workload Metrics

To quantitatively evaluate the workload for the user we introduce the following metrics: (1)  $NoI$  (lower is better) to denote the total number of user-corrections issued by the model to refine its current prediction. (2)  $\Delta I$  (higher is better), is introduced as an intuitive metric that reports the average time between two user-corrections reported in seconds. Note that some sequences might have no user interactions; however, to include every sequence in the evaluation, we consider the initialization and the end of a sequence as user-interactions. (3) As  $\Delta I$  does not reflect the underlying distribution of the interactions, we provide through  $\mathcal{N}_{\Delta I} \in [0, +\infty]$  (which encapsulates both  $NoI$  and  $\Delta I$ ) a score to indicate this distribution. In essence, we compute the cumulative count over user interactions and their respective distance to each other. Consequently, a low  $\mathcal{N}_{\Delta I} \in [0, +\infty]$  score indicates more dispersed consecutive interactions from each other, while a higher score indicates consecutive interactions more closer to each other. More formally, let  $\mathcal{N}_o = \{f_{p=0}, \dots, f_{p=P_o} \mid f_p \in F_o\}$  denote the set containing the frame indexes  $f_p$  where a user prompt  $p$  is issued for object  $o$ . Hence, we define  $\mathcal{N}_{\Delta I}$ , such that

$$\mathcal{N}_{\Delta I} = \sum_{o \in \mathcal{O}} \frac{1}{|F_o|} \sum_{i=1}^{|F_o|} \sum_{j=1}^i n_j, \quad (7)$$

where  $n_j = \sum_{f_p=1}^{\mathcal{N}_o} \mathbb{1}_{[j=f_p-f_{p-1}]}$  denotes the number of occurrences a user provided corrections at a distance of  $j$  frames from one prompt to the next. While  $\mathcal{N}_{\Delta I}$  loses practical interpretability compared to  $NoI$  and  $\Delta I$ , it provides a single metric for easier ranking.

## 4.3 Evaluation Framework

As our goal is to improve the robustness of video object segmentation methods by incorporating user corrections on-the-fly, while minimizing the user’s workload, we only allow one interaction per object per frame. Following standard practices only two form of interactions are possible, *i.e.*, positive and negative, to indicate foreground and background regions respectively. Moreover, we limit the type

of interactions to only clicks, as pointing an object is the quickest and most intuitive interaction type for humans [14, 18].

To automatically evaluate ziVOS methods, we simulate a user interaction  $u_f^o$  at frame  $f$  for object  $o$  in the sequence using a *simulated agent*, whenever the ziVOS method requests a user correction. We simulate an interaction at the center of a given region  $\mathcal{R}_f^o$  similarly to Eq. (4) and Eq. (5), but without weighting the results with the uncertainty map  $\mathbf{S}$ , and replacing the object  $\mathbf{M}_c$  and dilated  $\mathbf{M}_c^d$  masks with the ground-truth object mask  $\mathbf{GT}_f^o$ .

## 5 Experiments

In Section 5.1, we assess the effectiveness of the proposed masked entropy  $\mathcal{S}_{\mathcal{R}_c}$  to estimate the tracking’s state on-the-fly. Section 5.2 details our results (*i.e.*, Lazy-XMem) on the LVOS dataset [22], following the ziVOS approach (see Figure 1), and compares Lazy-XMem against State-of-the-Art (SotA) sVOS methods. Lastly, an ablation study in Section 5.3 examines the impact of each design choice.

### 5.1 Entropy as a Proxy

To evaluate the effectiveness of the masked entropy  $\mathcal{S}_{\mathcal{R}_c}$  to estimate the tracking’s state, we compare against the following approaches: (1) Using the Quality-Aware Module (QAM) from QDMN [38], which predicts a confidence score through an auxiliary network. (2) Computing the entropy  $S$  and its masked version  $\mathcal{S}_{\mathcal{R}}$  for various models: single models denoted as Q and X respectively for the QDMN [38] and XMem [8] networks, an ensemble model denoted as E, and a Monte-Carlo dropout model denoted as M. We provide in the supplementary material details to the ensemble and Monte Carlo dropout approaches. (3) We also consider for the ensemble and Monte-Carlo dropout variants the epistemic uncertainty, denoted as  $V$  (and the masked version  $V_{\mathcal{R}}$ ). For each method, we compute the Spearman coefficient [56] to measure the correlation between each variant’s output for the tracking state w.r.t. the actual IoU. We conduct our evaluations on the DAVIS 2017 [49] and LVOS [22] validation sets, featuring short and long videos respectively.

Figure 3 presents the distribution (*i.e.*, box-plots) of the correlation coefficients when computing the coefficient for every object present in a dataset. Aside from the QAM based methods, we expect an inverse correlation, however, to facilitate the comparison, we invert the correlation results for all methods except for the QAM version. Consequently, values closer to 1 indicate a higher correlation, suggesting a more accurate estimate of the tracking state. Across both the DAVIS 2017 [49] and LVOS [22] datasets, variants employing masked entropy (*i.e.*,  $\mathcal{S}_{\mathcal{R}}$ ) demonstrate notably stronger correlations. This highlights the effectiveness of isolating uncertainty at the object level using a mask. Among the different model variants – single (Q and X), ensemble (E), and Dropout (M)

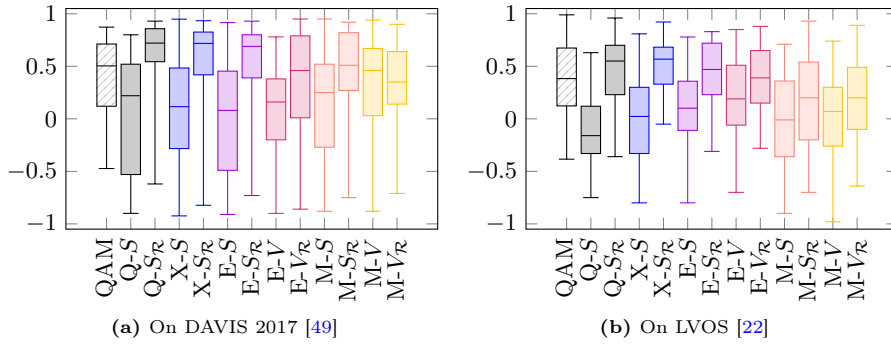


**Fig. 3:** Comparison of correlation coefficients across the DAVIS 2017 [49] and LVOS [22] datasets: i) the QAM module [38] and entropy based QDMN [38] (as Q-S and Q-S<sub>R</sub>), ii) entropy results for a single baseline (X-S, X-S<sub>R</sub>), an ensemble (E-S, E-S<sub>R</sub>), and Monte-Carlo methods (M-S, M-S<sub>R</sub>), and iii) epistemic uncertainty variants for ensemble and Monte-Carlo (E-V, E-V<sub>R</sub>, M-V, M-V<sub>R</sub>).

– the single models (Q and X) leveraging  $S_{\mathcal{R}}$  outperform even the advanced learning-based QAM module [38].

Hence, by examining Figure 3, the most effective method for estimating the tracking state on-the-fly appears to be the masked entropy approach, particularly the X-S<sub>R</sub> variant, as its median value is closer to 1 and the distribution is notably narrower. This underscores the efficacy of masked entropy as a straightforward yet robust approach to estimate the tracking’s state on-the-fly.

## 5.2 Quantitative Results

In Table 1, we present quantitative results of Lazy-XMem compared w.r.t. SotA methods on the LVOS validation set [22]. Following the proposed ziVOS framework, we initialize each method (which objects to segment in the video) through simulated click as described in Section 4.3. Hence, unlike sVOS, which initializes object of interests with curated masks, we employ imperfect object masks generated by the mask refiner (*i.e.*, SAM-HQ [29]). We also provide results when initializing the methods with the curated masks (*i.e.*, as in sVOS) in the supplementary material. To allow for a better comparability, we also evaluate a modified version of QDMN [38], that adopts the same design as LazyXMem for integrating user and pseudo-corrections, with the notable exception that the tracking state estimation is based on the QAM module [38]. Moreover, we evaluate an alternative approach that simply requests user corrections at random intervals throughout the sequence (denoted as Rand-Lazy-XMem). In addition, we introduce a variant of Lazy-XMem (denoted by Lazy-XMem<sup>†</sup>), which operates without user corrections to facilitate the comparison w.r.t. SotA sVOS methods. We report the popular  $\mathcal{J}\&\mathcal{F}$  metric, alongside our complementary metrics (as discussed in Section 4).

**Table 1:** Quantitative evaluation of ziVOS and sVOS methods on the LVOS validation set [22] following the ziVOS framework. Here, we initialize each methods with an imperfect mask, in contrast to sVOS, to indicate which object to segment in the sequence.

Method	$\mathcal{J}\&\mathcal{F}$	Robustness			User-Workload		
		$R@0.1$	$R@0.25$	$R@0.5$	$\mathcal{N}_{\Delta\mathcal{I}}$	$No\mathcal{I}$	$\Delta\mathcal{I}$
<i>sVOS Methods</i>							
QDMN [38] (ECCV 2022)	44.2	47.8	45.5	36.2	$\times$	$\times$	$\times$
XMem [8] (ECCV 2022)	52.8	57.0	55.0	49.0	$\times$	$\times$	$\times$
DEVA [7] (ICCV 2023)	55.1	63.6	59.3	52.4	$\times$	$\times$	$\times$
Cutie-base [6] (CVPR 2024)	57.0	59.2	57.8	52.4	$\times$	$\times$	$\times$
Cutie-small [6] (CVPR 2024)	57.6	58.6	57.0	52.5	$\times$	$\times$	$\times$
Lazy-XMem <sup>†</sup> (ours)	56.4	58.8	56.8	50.6	$\times$	$\times$	$\times$
<i>ziVOS Methods</i>							
Rand-Lazy-XMem	61.3	67.9	65.8	59.3	5.17	335	17.9
Lazy-QDMN	52.7	58.2	52.0	42.9	5.64	360	16.7
Lazy-XMem (ours)	64.3	70.2	67.8	62.3	5.02	325	18.4

As shown in Table 1, our proposed Lazy-XMem<sup>†</sup> achieves competitive results w.r.t. to the SotA sVOS methods. However the robustness is still close to the original XMem [8] version, despite of the increase in accuracy. By incorporating user corrections (*i.e.*, Lazy-XMem), we manage to improve the robustness by 13 points on average over all robustness metrics, while requesting in total 325 interactions from the user for the entire datasets, averaging one interaction every 18.4 seconds. This corresponds to approximately 1.05% of the total number of frames in the LVOS validation set, which contains 30,876 frames [22].

While Lazy-XMem incorporates user corrections on-the-fly to enhance its robustness, it requires a continuous participation of the user throughout the segmentation process. Therefore, we present Lazy-XMem as an alternative to sVOS and iVOS methods to segment offline and online videos, in scenarios where user engagement is feasible and where segmenting over an extended period with high reliability is the priority.

### 5.3 Ablations

To provide more insights into our pipeline, we detail the influence of each design choice in Table 2.

Using the Uncertainty Driven Update (UDU), we achieve improvements over the baseline by selectively integrating memory predictions that present sufficiently low uncertainty. By soliciting user interactions to refine the initial mask predicted by the sVOS baseline (*i.e.*, XMem [8]), we achieve slight improvements at the cost of 507 interactions across the dataset. While, storing the refined masks as references for future segmentation after a user correction through the Interaction Driven Update (IDU), we attain substantial improvements in both

**Table 2:** Ablation study for Lazy-XMem on the ziVOS framework. Here \* denotes using the original mask of the sVOS baseline as an additional prompt to the mask refiner. We initialize each method with an imperfect mask, to indicate which object to segment in the sequence.

Configuration	$\mathcal{J}\&\mathcal{F}$	Robustness			User-Workload		
		$R@0.1$	$R@0.25$	$R@0.5$	$\mathcal{N}_{\Delta\mathcal{I}}$	$No\mathcal{I}$	$\Delta\mathcal{I}$
XMem [8] (baseline)	52.8	57.0	55.0	49.0	$\times$	$\times$	$\times$
<i>+ Uncertainty Driven Updates (UDU)</i>							
XMem-UDU	54.7	56.3	54.5	50.0	$\times$	$\times$	$\times$
<i>+ User Corrections</i>							
XMem-UDU	55.6	58.2	56.4	51.8	7.80	507	12.6
XMem-UDU-IDU	62.9	67.8	66.2	60.9	5.05	327	18.3
XMem-UDU-IDU*	48.4	57.5	53.9	48.2	4.30	279	20.9
<i>+ Pseudo Corrections</i>							
Lazy-XMem	64.3	70.2	67.8	62.3	5.02	325	18.4
Lazy-XMem + pseudo-IDU	64.3	70.1	68.2	62.1	5.91	352	17.3
<i>- User Corrections</i>							
Lazy-XMem <sup>†</sup>	56.4	58.8	56.8	50.6	$\times$	$\times$	$\times$
Lazy-XMem <sup>†</sup> + pseudo-IDU	53.1	57.0	55.1	49.6	$\times$	$\times$	$\times$

robustness and user workload. However, using the original mask from XMem [8], associated with a high uncertainty, as an additional prompt to the user’s interaction for the mask refiner leads to a decrease in performance.

By generating pseudo-interactions following the strategy outlined in Section 3.4 to refine XMem’s initial mask, we enhance the robustness even further while slightly reducing the user’s workload. However, saving the resulting refined mask from a pseudo-interaction (termed pseudo-IDU), affect only marginally the robustness, but increases the user workload considerably. When discarding the user interactions and only relying on pseudo-corrections, *i.e.*, Lazy-XMem<sup>†</sup>, we obtain a similar setup to sVOS methods and manage to improve the results of the XMem [8] baseline, even attain competitive results against the current SotA sVOS methods as shown in Table 1.

## 6 Conclusion

We introduce Lazy-XMem as a reference for future work tackling ziVOS, a hybrid combination of sVOS and iVOS, that emulates a human-in-the-loop process for online video segmentation. Through Lazy-XMem, we enhance the robustness (*i.e.*, the ratio of frames segmented above a certain IoU threshold) w.r.t. the sVOS baseline (*i.e.*, XMem [8]) by integrating pseudo and user corrections on-the-fly. However, as we solicit user corrections, we also aim to reduce the user’s workload, striking a balance between performance and user engagement by requesting help only during critical events, where the method is likely to fail. We

estimate the tracking state (*i.e.*, confidence) of the method by leveraging entropy (from information theory) and demonstrate that our proposed approach is an effective means of estimating the tracking state on-the-fly. As we propose ziVOS, we also introduce complementary metrics to the popular  $\mathcal{J}\&\mathcal{F}$  metrics [47], to evaluate the robustness of our approach and the user’s workload. Our evaluation on the long-term LVOS dataset [22] shows that Lazy-XMem improves the robustness relative to the baseline, albeit at the cost of additional user interactions. Thus, we present Lazy-XMem as an alternative to sVOS and iVOS methods to segment online video, particularly when on-the-fly corrections by a user are possible and when maintaining the tracking for an extended period is preferred over the accuracy of a method.

## References

1. Athar, A., Luiten, J., Voigtlaender, P., Khurana, T., Dave, A., Leibe, B., Ramanan, D.: Burst: A benchmark for unifying object recognition, segmentation and tracking in video. In: Winter Conference on Applications of Computer Vision (WACV) (2023) 4
2. Bekuzarov, M., Bermudez, A., Lee, J.Y., Li, H.: Xmem++: Production-level video segmentation from few annotated frames (2023) 2, 4
3. Benard, A., Gygli, M.: Interactive video object segmentation in the wild. arXiv preprint arXiv:1801.00269 (2017) 5
4. Caelles, S., Maninis, K.K., Pont-Tuset, J., Leal-Taixé, L., Cremers, D., Van Gool, L.: One-shot video object segmentation. In: Conference on Computer Vision and Pattern Recognition (CVPR) (2017) 3
5. Caelles, S., Montes, A., Maninis, K.K., Chen, Y., Van Gool, L., Perazzi, F., Pont-Tuset, J.: The 2018 davis challenge on video object segmentation. arXiv:1803.00557 (2018) 4
6. Cheng, H.K., Oh, S.W., Price, B., Lee, J.Y., Schwing, A.: Putting the object back into video object segmentation. In: Conference on Computer Vision and Pattern Recognition (CVPR) (2024) 2, 4, 13, 21
7. Cheng, H.K., Oh, S.W., Price, B., Schwing, A., Lee, J.Y.: Tracking anything with decoupled video segmentation. In: International Conference on Computer Vision (ICCV) (2023) 13, 21
8. Cheng, H.K., Schwing, A.G.: XMem: Long-term video object segmentation with an atkinson-shiffrin memory model. In: European Conference on Computer Vision (ECCV) (2022) 2, 4, 6, 7, 11, 13, 14, 21, 22
9. Cheng, H.K., Tai, Y.W., Tang, C.K.: Modular interactive video object segmentation: Interaction-to-mask, propagation and difference-aware fusion. In: Conference on Computer Vision and Pattern Recognition (CVPR) (2021) 4, 5, 6, 22
10. Cheng, H.K., Tai, Y.W., Tang, C.K.: Rethinking space-time networks with improved memory coverage for efficient video object segmentation. In: Neural Information Processing Systems (NeurIPS) (2021) 4, 6, 22
11. Cheng, Y., Li, L., Xu, Y., Li, X., Yang, Z., Wang, W., Yang, Y.: Segment and track anything. arXiv preprint arXiv:2305.06558 (2023) 4
12. Cho, K., Van Merriënboer, B., Gulcehre, C., Bahdanau, D., Bougares, F., Schwenk, H., Bengio, Y.: Learning phrase representations using rnn encoder-decoder for statistical machine translation. Conference on Empirical Methods in Natural Language Processing (EMNLP) (2014) 7

13. Cho, S., Lee, H., Lee, M., Park, C., Jang, S., Kim, M., Lee, S.: Tackling background distraction in video object segmentation. In: European Conference on Computer Vision (ECCV) (2022) [4](#)
14. Clark, H.H.: Coordinating with each other in a material world. *Discourse studies* (2005) [2](#), [11](#)
15. Delatolas, T., Kalogeiton, V., Papadopoulos, D.P.: Learning the what and how of annotation in video object segmentation. In: Winter Conference on Applications of Computer Vision (WACV) (2024) [3](#), [5](#), [26](#)
16. Ding, H., Liu, C., He, S., Jiang, X., Torr, P.H., Bai, S.: MOSE: A new dataset for video object segmentation in complex scenes. In: International Conference on Computer Vision (ICCV) (2023) [4](#), [22](#)
17. Dupont, C., Ouakrim, Y., Pham, Q.C.: Ucp-net: Unstructured contour points for instance segmentation. *arXiv preprint arXiv:2109.07592* (2021) [4](#)
18. Firestone, C., Scholl, B.J.: “please tap the shape, anywhere you like” shape skeletons in human vision revealed by an exceedingly simple measure. *Psychological science* (2014) [2](#), [11](#)
19. Forte, M., Price, B., Cohen, S., Xu, N., Pitié, F.: Getting to 99% accuracy in interactive segmentation. *arXiv preprint arXiv:2003.07932* (2020) [4](#)
20. Heo, Y., Jun Koh, Y., Kim, C.S.: Interactive video object segmentation using global and local transfer modules. In: European Conference on Computer Vision (ECCV) (2020) [5](#)
21. Heo, Y., Koh, Y.J., Kim, C.S.: Guided interactive video object segmentation using reliability-based attention maps. In: Conference on Computer Vision and Pattern Recognition (CVPR) (2021) [5](#)
22. Hong, L., Chen, W., Liu, Z., Zhang, W., Guo, P., Chen, Z., Zhang, W.: Lvos: A benchmark for long-term video object segmentation. In: Proceedings of the IEEE/CVF International Conference on Computer Vision (ICCV) (2023) [2](#), [3](#), [4](#), [11](#), [12](#), [13](#), [15](#), [21](#), [22](#), [24](#), [25](#), [27](#), [28](#)
23. Hu, P., Wang, G., Kong, X., Kuen, J., Tan, Y.P.: Motion-guided cascaded refinement network for video object segmentation. In: Conference on Computer Vision and Pattern Recognition (CVPR) (2018) [3](#)
24. Huang, Z., Huang, L., Gong, Y., Huang, C., Wang, X.: Mask Scoring R-CNN. In: Conference on Computer Vision and Pattern Recognition (CVPR) (2019) [3](#)
25. Jain, S., Grauman, K.: Click carving: Segmenting objects in video with point clicks. In: Association for the Advancement of Artificial Intelligence (AAAI) (2016) [5](#)
26. Jang, W.D., Kim, C.S.: Online video object segmentation via convolutional trident network. In: Conference on Computer Vision and Pattern Recognition (CVPR) (2017) [3](#)
27. Jang, W.D., Kim, C.S.: Interactive image segmentation via backpropagating refinement scheme. In: Conference on Computer Vision and Pattern Recognition (CVPR) (2019) [4](#)
28. Johnander, J., Danelljan, M., Brissman, E., Khan, F.S., Felsberg, M.: A generative appearance model for end-to-end video object segmentation. In: Conference on Computer Vision and Pattern Recognition (CVPR) (2019) [3](#)
29. Ke, L., Ye, M., Danelljan, M., Liu, Y., Tai, Y.W., Tang, C.K., Yu, F.: Segment anything in high quality. In: Neural Information Processing Systems (NeurIPS) (2023) [3](#), [4](#), [8](#), [12](#)
30. Kirillov, A., Mintun, E., Ravi, N., Mao, H., Rolland, C., Gustafson, L., Xiao, T., Whitehead, S., Berg, A.C., Lo, W.Y., Dollár, P., Girshick, R.: Segment anything. *arXiv:2304.02643* (2023) [4](#), [8](#)



31. Kontogianni, T., Gygli, M., Uijlings, J., Ferrari, V.: Continuous adaptation for interactive object segmentation by learning from corrections. In: European Conference on Computer Vision (ECCV) (2020) [4](#)
32. Kristan, M., et al.: The first visual object tracking segmentation vots2023 challenge results. In: International Conference on Computer Vision Workshops (ICCVW) (2023) [4](#), [9](#), [10](#)
33. Li, M., Hu, L., Xiong, Z., Zhang, B., Pan, P., Liu, D.: Recurrent dynamic embedding for video object segmentation. In: Conference on Computer Vision and Pattern Recognition (CVPR) (2022) [4](#)
34. Li, Y., Shen, Z., Shan, Y.: Fast video object segmentation using the global context module. In: European Conference on Computer Vision (ECCV) (2020) [4](#)
35. Li, Z., Chen, Q., Koltun, V.: Interactive image segmentation with latent diversity. In: Conference on Computer Vision and Pattern Recognition (CVPR) (2018) [4](#)
36. Liang, Y., Li, X., Jafari, N., Chen, J.: Video object segmentation with adaptive feature bank and uncertain-region refinement. In: Neural Information Processing Systems (NeurIPS) (2020) [2](#), [4](#), [7](#)
37. Liu, Y., Yu, R., Wang, J., Zhao, X., Wang, Y., Tang, Y., Yang, Y.: Global spectral filter memory network for video object segmentation. In: European Conference on Computer Vision (ECCV) (2022) [4](#)
38. Liu, Y., Yu, R., Yin, F., Zhao, X., Zhao, W., Xia, W., Yang, Y.: Learning quality-aware dynamic memory for video object segmentation. In: European Conference on Computer Vision (ECCV) (2022) [2](#), [3](#), [4](#), [5](#), [9](#), [11](#), [12](#), [13](#), [21](#)
39. Maninis, K.K., Caelles, S., Chen, Y., Pont-Tuset, J., Leal-Taixé, L., Cremers, D., Van Gool, L.: Video object segmentation without temporal information. Transactions on Pattern Analysis and Machine Intelligence (TPAMI) (2018) [3](#)
40. Maninis, K.K., Caelles, S., Pont-Tuset, J., Van Gool, L.: Deep extreme cut: From extreme points to object segmentation. In: Conference on Computer Vision and Pattern Recognition (CVPR) (2018) [4](#)
41. Marinov, Z., Jäger, P.F., Egger, J., Kleesiek, J., Stiefelwagen, R.: Deep interactive segmentation of medical images: A systematic review and taxonomy. arXiv preprint arXiv:2311.13964 (2023) [4](#)
42. Meinhardt, T., Leal-Taixé, L.: Make one-shot video object segmentation efficient again. Neural Information Processing Systems (NeurIPS) (2020) [3](#)
43. Miao, J., Wei, Y., Yang, Y.: Memory aggregation networks for efficient interactive video object segmentation. In: Conference on Computer Vision and Pattern Recognition (CVPR) (2020) [5](#)
44. Oh, S.W., Lee, J.Y., Xu, N., Kim, S.J.: Fast user-guided video object segmentation by interaction-and-propagation networks. In: Conference on Computer Vision and Pattern Recognition (CVPR) (2019) [5](#)
45. Oh, S.W., Lee, J.Y., Xu, N., Kim, S.J.: Video object segmentation using space-time memory networks. In: International Conference on Computer Vision (ICCV) (2019) [4](#), [6](#), [7](#)
46. Park, K., Woo, S., Oh, S.W., Kweon, I.S., Lee, J.Y.: Per-clip video object segmentation. In: Conference on Computer Vision and Pattern Recognition (CVPR) (2022) [4](#)
47. Perazzi, F., Pont-Tuset, J., McWilliams, B., Van Gool, L., Gross, M., Sorkine-Hornung, A.: A benchmark dataset and evaluation methodology for video object segmentation. In: Conference on Computer Vision and Pattern Recognition (CVPR) (2016) [3](#), [9](#), [15](#)

48. Perazzi, F., Khoreva, A., Benenson, R., Schiele, B., Sorkine-Hornung, A.: Learning video object segmentation from static images. In: Conference on Computer Vision and Pattern Recognition (CVPR) (2017) [3](#)
49. Pont-Tuset, J., Perazzi, F., Caelles, S., Arbeláez, P., Sorkine-Hornung, A., Van Gool, L.: The 2017 davis challenge on video object segmentation. arXiv:1704.00675 (2017) [2](#), [4](#), [11](#), [12](#), [22](#)
50. Rother, C., Kolmogorov, V., Blake, A.: " grabcut" interactive foreground extraction using iterated graph cuts. ACM transactions on graphics (TOG) (2004) [4](#)
51. Seong, H., Hyun, J., Kim, E.: Kernelized memory network for video object segmentation. In: European Conference on Computer Vision (ECCV) (2020) [4](#)
52. Seong, H., Oh, S.W., Lee, J.Y., Lee, S., Lee, S., Kim, E.: Hierarchical memory matching network for video object segmentation. In: International Conference on Computer Vision (ICCV) (2021) [4](#)
53. Shannon, C.E.: A mathematical theory of communication. The Bell system technical journal (1948) [3](#), [5](#), [7](#)
54. Sofiuk, K., Petrov, I., Barinova, O., Konushin, A.: f-brs: Rethinking backpropagating refinement for interactive segmentation. In: Conference on Computer Vision and Pattern Recognition (CVPR) (2020) [4](#)
55. Sofiuk, K., Petrov, I.A., Konushin, A.: Reviving iterative training with mask guidance for interactive segmentation. In: International Conference on Image Processing (ICIP) (2022) [4](#)
56. Spearman, C.: The proof and measurement of association between two things. American Journal of Psychology (1904) [11](#)
57. Tompson, J., Goroshin, R., Jain, A., LeCun, Y., Bregler, C.: Efficient object localization using convolutional networks. In: Proceedings of the IEEE conference on computer vision and pattern recognition (CVPR) (2015) [22](#)
58. Voigtlaender, P., Chai, Y., Schroff, F., Adam, H., Leibe, B., Chen, L.C.: Feelvos: Fast end-to-end embedding learning for video object segmentation. In: Conference on Computer Vision and Pattern Recognition (CVPR) (2019) [4](#)
59. Voigtlaender, P., Leibe, B.: Online adaptation of convolutional neural networks for video object segmentation. British Machine Vision Conference (BMVC) (2017) [3](#)
60. Vujasinovic, S., Bullinger, S., Becker, S., Scherer-Negenborn, N., Arens, M., Stiefel-hagen, R.: Readmem: Robust embedding association for a diverse memory in unconstrained video object segmentation. In: British Machine Vision Conference (BMVC) (2023) [2](#), [4](#)
61. Vujasinović, S., Bullinger, S., Becker, S., Scherer-Negenborn, N., Arens, M., Stiefel-hagen, R.: Revisiting click-based interactive video object segmentation. In: International Conference on Image Processing (ICIP) (2022) [5](#)
62. Wang, J., Sun, K., Cheng, T., Jiang, B., Deng, C., Zhao, Y., Liu, D., Mu, Y., Tan, M., Wang, X., et al.: Deep high-resolution representation learning for visual recognition. Transactions on Pattern Analysis and Machine Intelligence (TPAMI) (2020) [4](#)
63. Wang, T., Han, B., Collomosse, J.P.: Touchcut: Fast image and video segmentation using single-touch interaction. Computer Vision and Image Understanding (CVIU) (2014) [5](#)
64. Wu, J., Zhao, Y., Zhu, J.Y., Luo, S., Tu, Z.: Milcut: A sweeping line multiple instance learning paradigm for interactive image segmentation. In: Conference on Computer Vision and Pattern Recognition (CVPR) (2014) [4](#)
65. Xiao, H., Feng, J., Lin, G., Liu, Y., Zhang, M.: Monet: Deep motion exploitation for video object segmentation. In: Conference on Computer Vision and Pattern Recognition (CVPR) (2018) [3](#)

66. Xiao, H., Kang, B., Liu, Y., Zhang, M., Feng, J.: Online meta adaptation for fast video object segmentation. *Transactions on Pattern Analysis and Machine Intelligence (TPAMI)* (2019) 3
67. Xie, H., Yao, H., Zhou, S., Zhang, S., Sun, W.: Efficient regional memory network for video object segmentation. In: *Conference on Computer Vision and Pattern Recognition (CVPR)* (2021) 4
68. Xu, N., Price, B., Cohen, S., Yang, J., Huang, T.: Deep grabcut for object selection. *arXiv preprint arXiv:1707.00243* (2017) 4
69. Xu, N., Price, B., Cohen, S., Yang, J., Huang, T.S.: Deep interactive object selection. In: *Conference on Computer Vision and Pattern Recognition (CVPR)* (2016) 4
70. Xu, N., Yang, L., Fan, Y., Yue, D., Liang, Y., Yang, J., Huang, T.: Youtube-vos: A large-scale video object segmentation benchmark. *arXiv preprint arXiv:1809.03327* (2018) 2, 4
71. Yang, J., Gao, M., Li, Z., Gao, S., Wang, F., Zheng, F.: Track anything: Segment anything meets videos (2023) 4
72. Yang, Z., Wei, Y., Yang, Y.: Collaborative video object segmentation by foreground-background integration. In: *European Conference on Computer Vision (ECCV)* (2020) 4
73. Yang, Z., Wei, Y., Yang, Y.: Associating objects with transformers for video object segmentation. In: *Neural Information Processing Systems (NeurIPS)* (2021) 4
74. Yang, Z., Wei, Y., Yang, Y.: Collaborative video object segmentation by multi-scale foreground-background integration. *Transactions on Pattern Analysis and Machine Intelligence (TPAMI)* (2021) 4
75. Yang, Z., Yang, Y.: Decoupling features in hierarchical propagation for video object segmentation. In: *Neural Information Processing Systems (NeurIPS)* (2022) 2, 4
76. Yin, Z., Zheng, J., Luo, W., Qian, S., Zhang, H., Gao, S.: Learning to recommend frame for interactive video object segmentation in the wild. In: *Conference on Computer Vision and Pattern Recognition (CVPR)* (2021) 3, 5
77. Yuan, Y., Chen, X., Chen, X., Wang, J.: Segmentation transformer: Object-contextual representations for semantic segmentation. In: *European Conference on Computer Vision (ECCV)* (2021) 4
78. Yunyao, M., Ning, W., Wengang, Z., Houqiang, L.: Joint inductive and transductive learning for video object segmentation. In: *International Conference on Computer Vision (ICCV)* (2021) 4
79. Zhang, C., Han, D., Qiao, Y., Kim, J.U., Bae, S.H., Lee, S., Hong, C.S.: Faster segment anything: Towards lightweight sam for mobile applications. *arXiv preprint arXiv:2306.14289* (2023) 4
80. Zhang, C., Liu, L., Cui, Y., Huang, G., Lin, W., Yang, Y., Hu, Y.: A comprehensive survey on segment anything model for vision and beyond. *arXiv:2305.08196* (2023) 4
81. Zhang, L., Lin, Z., Zhang, J., Lu, H., He, Y.: Fast video object segmentation via dynamic targeting network. In: *International Conference on Computer Vision (ICCV)* (2019) 3
82. Zhang, S., Liew, J.H., Wei, Y., Wei, S., Zhao, Y.: Interactive object segmentation with inside-outside guidance. In: *Conference on Computer Vision and Pattern Recognition (CVPR)* (2020) 4
83. Zhao, X., Ding, W., An, Y., Du, Y., Yu, T., Li, M., Tang, M., Wang, J.: Fast segment anything (2023) 4

84. Zhou, T., Porikli, F., Crandall, D.J., Van Gool, L., Wang, W.: A survey on deep learning technique for video segmentation. Transactions on Pattern Analysis and Machine Intelligence (TPAMI) (2023) [1](#), [3](#)
85. Zhu, J., Chen, Z., Hao, Z., Chang, S., Zhang, L., Wang, D., Lu, H., Luo, B., He, J.Y., Lan, J.P., Chen, H., Li, C.: Tracking anything in high quality (2023) [4](#)

# *SUPPLEMENTARY MATERIAL*

## Strike the Balance: On-the-Fly Uncertainty based User Interactions for Long-Term Video Object Segmentation

In this supplementary document we provide additional quantitative and qualitative experiments alongside insights on the current limitation and future directions for improvements.

### A Additional Evaluations

#### A.1 Quantitative Results (Perfect Mask Initialization)

Table S1 reports the evaluation of sVOS and ziVOS methods on the LVOS validation set [22], using ground-truth annotations to indicate which object to segment in the sequence (as in sVOS). We re-evaluated each method, and compute the robustness metric  $R@_{\tau IoU}$ , except for DDMemory [22] as the code is unavailable at the time of writing. Similarly to Table 1 (refer to the paper), Lazy-XMem<sup>†</sup> with only pseudo-interaction achieves competitive results to SotA sVOS methods. However, by including user interactions on-the-fly to aid Lazy-XMem, we manage to improve the results robustness for the cost of 315 interactions (about 1.02% of the total number of frames in LVOS).

**Table S1:** Quantitative evaluation of sVOS and ziVOS methods on the LVOS validation set [22], when initialized with the ground-truth annotations (curated masks as in sVOS).

Method	$\mathcal{J}\&\mathcal{F}$	Robustness			User-Workload		
		$R@0.1$	$R@0.25$	$R@0.5$	$\mathcal{N}_{\Delta\mathcal{I}}$	$\mathcal{N}_{o\mathcal{I}}$	$\Delta\mathcal{I}$
<i>sVOS</i>							
QDMN [38] (ECCV 2022)	48.2	54.0	50.1	41.5	$\times$	$\times$	$\times$
XMem [8] (ECCV 2022)	53.7	54.6	51.7	41.3	$\times$	$\times$	$\times$
DDMemory [22] (ICCV 2023)	60.7	$\times$	$\times$	$\times$	$\times$	$\times$	$\times$
DEVA [7] (ICCV 2023)	58.2	65.3	62.7	56.8	$\times$	$\times$	$\times$
Cutie-base [6] (CVPR 2024)	60.3	62.9	62.0	58.3	$\times$	$\times$	$\times$
Cutie-small [6] (CVPR 2024)	59.0	61.3	59.0	56.5	$\times$	$\times$	$\times$
Lazy-XMem (ours)	57.2	60.3	58.5	49.6	$\times$	$\times$	$\times$
<i>ziVOS</i>							
Rand-Lazy-XMem (ours)	60.3	66.3	64.3	58.8	5.05	320	18.2
Lazy-XMem (ours)	63.5	70.0	68.3	63.1	4.86	315	18.9

## A.2 Additional Ablations

Table S2 tabulates the results when relying directly on the masked entropy  $S_{\mathcal{R}_c}$  and its respective derivative  $\Delta S_{\mathcal{R}_c}$  as a condition to request user help. To isolate the influence each strategy for calling the user’s help, we discard the mask refiner and the pseudo interaction. We only consider user interactions and rely directly on the ground-truth annotations to correct the model’s predictions, instead of the mask refiner. We can see in table Table S2, that both strategies enhance the robustness and the accuracy, especially when updating the memory of the sVOS baseline (XMem [8]) with the refined masks through the Interaction Driven Update (IDU). However, by issuing an interaction based on the derivative  $S_{\mathcal{R}_c}$ , we manage to significantly reduce the number of user calls from 787 to 327 calls

**Table S2:** Results for Lazy-XMem when requesting user corrections through  $S_{\mathcal{R}_c}$  or  $\Delta S_{\mathcal{R}_c}$  (note that for this table we discard the pseudo-interaction). We initialize each method with perfect masks. UDU denotes Uncertainty Driven Update

Configuration	$\mathcal{J}\&\mathcal{F}$	Robustness			User-Workload		
		$R@0.1$	$R@0.25$	$R@0.5$	$\mathcal{N}_{\Delta\mathcal{I}}$	$No\mathcal{I}$	$\Delta\mathcal{I}$
XMem [8] (baseline)	53.7	54.6	51.7	41.3	<b>X</b>	<b>X</b>	<b>X</b>
<i>Call user corrections based on <math>S_{\mathcal{R}_c}</math></i>							
XMem + UDU	54.7	56.3	54.5	50.0	56.1	3647	1.9
XMem + UDU + IDU	63.5	67.6	66.1	61.7	12.1	787	8.5
<i>Call user corrections based on <math>\Delta S_{\mathcal{R}_c}</math></i>							
XMem + UDU	55.6	58.2	56.4	51.8	7.80	507	12.6
XMem + UDU + IDU	62.9	67.8	66.2	60.9	5.05	327	18.3

## B Implementation Details

For our sVOS baseline, we rely on the original weights provided by the authors of XMem [8], which is trained on the static and DAVIS 2017 training set [49]

**Deep Ensemble variant:** We experiment with an ensemble approach that combines three XMem models. The first model is trained on the static [10] and DAVIS 2017 training set [49]. The second model (which we use as a baseline in Lazy-XMem) is trained similarly to the first model but also includes the synthetic dataset BL30K [9]. The third model is trained like the first model but with the addition of the MOSE [16] dataset.

**Monte Carlo variant:** We rely on spatial pooling [57] applied to the key-projection of XMem [?], with a dropout ratio of 0.2 for our Monte Carlo Dropout variant during training, which is maintained during inference. For more details, we refer the reader to the original paper [8].

**Thresholds:** We using the training set of the LVOS dataset [22] to identify the values for  $\tau_u = 0.5$ ,  $\tau_p = 0.2$  and  $\tau_m = 0.8$ .

**Hardware:** All experiments are performed on an Nvidia GeForce GTX 1080 Ti.

## C Qualitative Results

In this section we provide qualitative results that highlight both success and failure cases whenever Lazy-XMem issues either pseudo- or user-corrections to generate a refined mask. Figure S1 and Figure S2 displays success and failure cases, respectively, for generating a refined mask through pseudo-corrections. Figure S3 and Figure S4 show results when a refined mask is generated via a simulated user-correction, as described in Section 4.3.

We indicate a ground-truth mask in yellow, the original prediction in turquoise, the refined mask in orange or purple after a pseudo- and user-correction respectively. We mark the location of a pseudo- or user-corrections through a yellow star ★.

For small objects, we provide a cropped version to better visualize the different predictions. In these cases, a small image of the original image is shown on the first column, surrounded by a red border. Note that in Figure S4, we do not display refined masks for the third, fourth and fifth rows, as Lazy-XMem missed for those instances the generation of either a user- or pseudo-corrections.

### C.1 Pseudo-Corrections

Through the pixel wise uncertainty estimation, we are able to identify confusing and confident regions, helpful for the generation of pseudo-corrections, allowing us to correct the segmentation whenever a distractors is present and anticipate when the method is likely to fail as shown in Figure S1. We can observe that our proposed pseudo-correction generation strategy successfully recovers the original object of interest in the presence of distractors (e.g., rows two, three, and four). Additionally, objects that are about to be lost are also recovered (e.g., rows one, three, and five).

Note that for small objects (refer to Figure S2), the mask refinement incorrectly generates masks, although the pseudo-correction location’s lies on the target, as seen in rows two, three, and five. In the first row, the small gorilla (target) is lost in favor to the adult gorilla, since the uncertainty is lower the method fails to issue correct pseudo-corrections or request a user-corrections. Ideally, the method should detect the transition from the small gorilla to the adult gorilla, while the pixel level uncertainty for both objects is still high, to indicate confusion. In row 6, we note that the pixel uncertainty for the foot region and the ball (target) are very similar, consequently the method is unable to find a correct location for the pseudo-correction generation as both object are as likely considered as the actual object to track by the sVOS baseline, here the method failed to actually issue a user-correction.



**Fig. S1:** Qualitative results on the validation set of LVOS [22] when refining the mask through pseudo-corrections (Success cases).



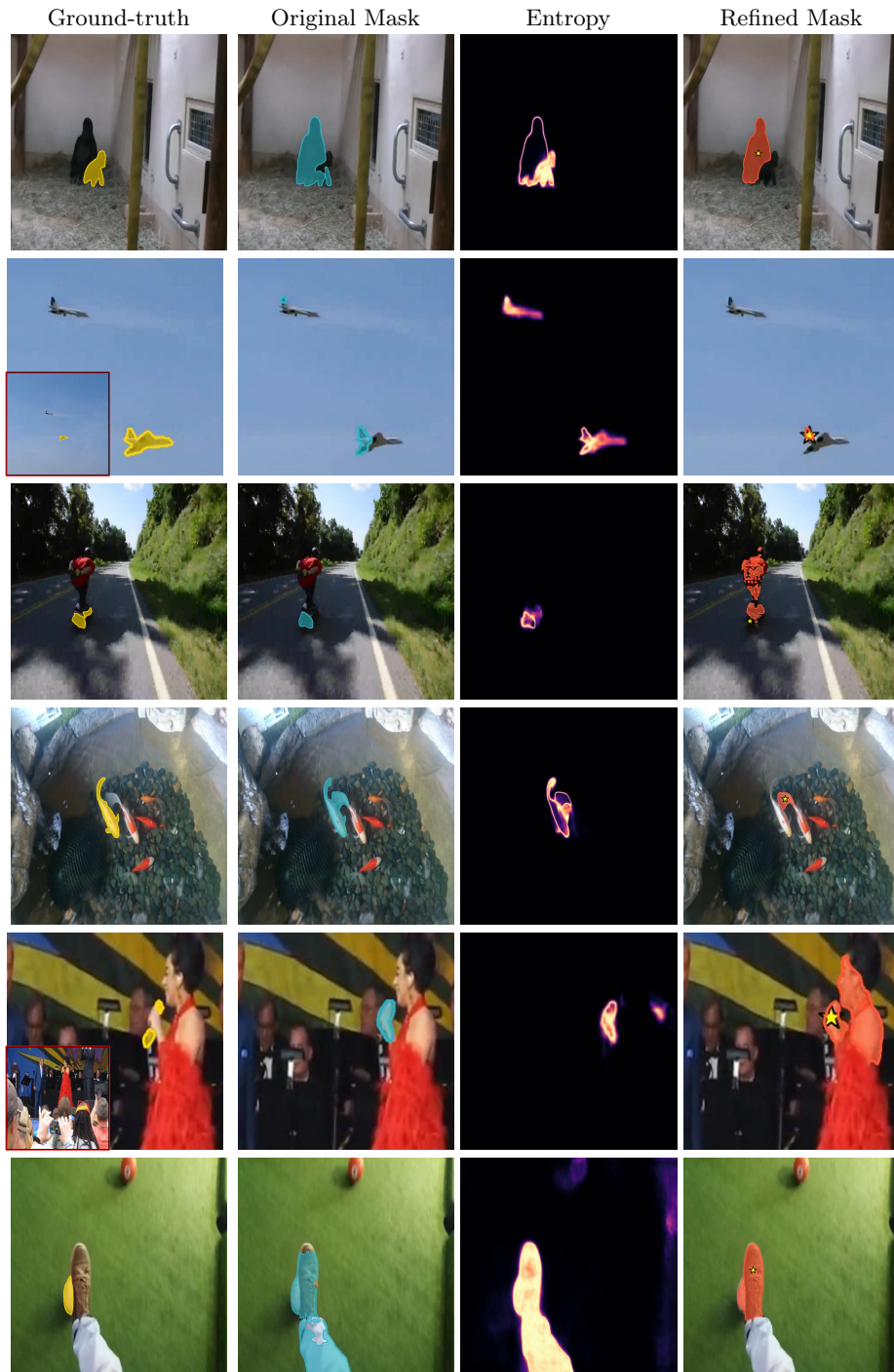


**Fig. S2:** Qualitative results on the validation set of LVOS [22] when refining the mask through pseudo-corrections (Failure cases).

## C.2 User-Corrections

In the first and last rows of Figure S3, we note that the method correctly issues a user interactions, as only the ear of the sheep and the back of the zebra are still segmented, preventing the loss of the target. Similarly, in the second and third rows, the method manages to issue and interaction to the user while losing the target in favor to a distractors. Note that in the third row, the method correctly issues a user-correction instead of a pseudo-correction, as otherwise the pseudo-correction would be generated on the wrong sheep.

In Figure S4, we observe that the method sometimes unnecessarily calls for user interaction even when a good portion of the object is correctly predicted (*i.e.*, first and second row), and where a pseudo-correction would be more appropriate (first row).

Additionally, there are instances where a user (or pseudo) correction is missed, as seen in rows three, four and five. In the fourth row, the tracker confidently segments a distractor after the disappearance of the object of interest, while indicating the actual object with some uncertainty. Lastly, when the SVOS backbone loses track of the object of interest, it is unable to recover it, as shown in the fifth row.

## D Limitations and Future Directions

Currently, Lazy-XMem generates only click-based pseudo-corrections, which are fed to the mask-refiner without including the predicted mask. This approach limits the impact of the initial mask proposed by the sVOS pipeline.

This bottleneck is inherent to SAM-based models, as they do not consider masks as prompts in practice. An alternative approach, explored by Delatolas *et al.* [15], involves iteratively prompting the mask-refiner with pseudo-prompts generated from the initial mask until a certain level of alignment is achieved between the SAM-predicted mask and the original sVOS initial mask. However, this method assumes that the initial mask (from the sVOS pipeline) is accurate enough to serve as a reliable base for further prompting the mask-refiner with uncertainty-based prompts.

An additional direction to follow in future work is to incorporate other types of prompts, like bounding-boxes or scribble-type, which might add more context to the prompt. Additionally, while we mostly rely on positive pseudo-clicks, including negative interactions could further enhance the method’s capabilities.

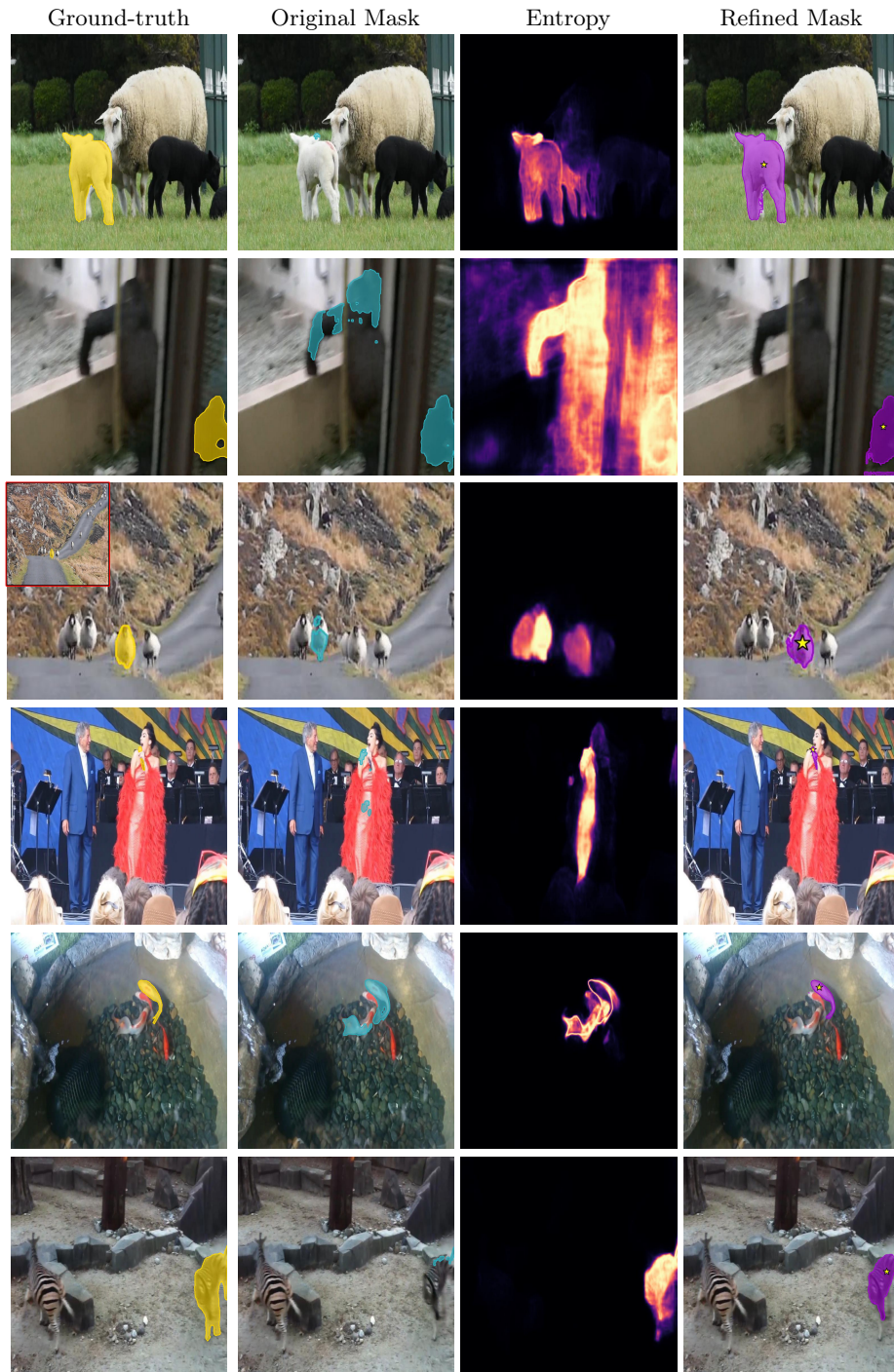


**Fig. S3:** Qualitative results on the validation set of LVOS [22] when refining the mask through user-corrections (Success cases).

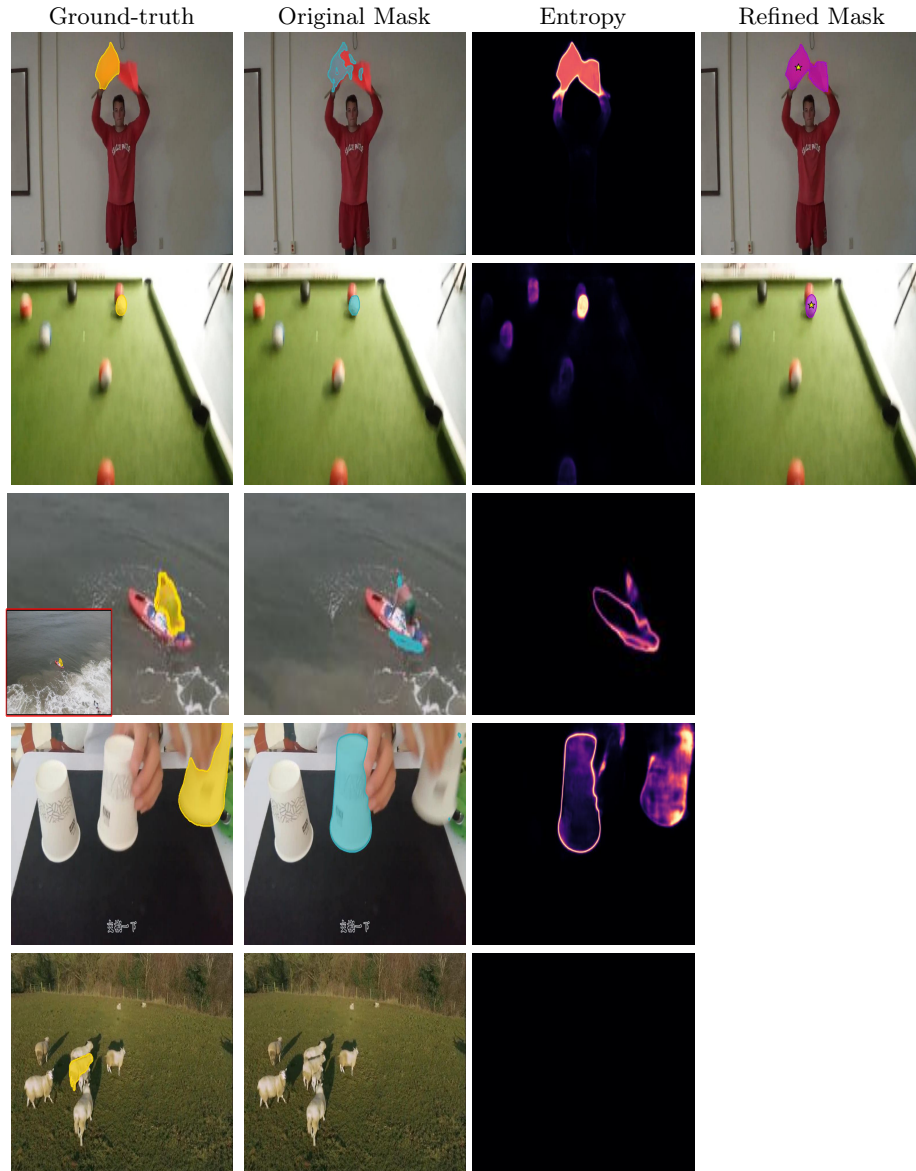


**Fig. S4:** Qualitative results on the validation set of LVOS [22] when refining the mask through user-corrections (Failure and miss cases). Here we considered a missed opportunity to generate a pseudo- or user-correction whenever the IoU between the original prediction and the ground-truth annotation is below 0.1.